A NOVEL TEMPLATE STAGE WITH SUPERIOR ALIGNMENT CAPABILITY FOR NANOIMPRINT AND STEP AND FLASH LITHOGRAPHPY

A Thesis

Submitted to the Graduate Faculty of the
Louisiana State University and
Agricultural and Mechanical College
in partial fulfillment of the
requirements for the degree of
Master of Science in Electrical Engineering

in

The Department of Electrical and Computer Engineering

by
Yunmi Jeon
B.S., Dong-A University, 2005
December 2007

ACKNOWLEDGMENTS

I appreciate all those who support and encourage me during this research from the bottom of my heart.

I would like to express my undying gratitude and respect to my advisor Dr. Martin Feldman for his invaluable and consistent guidance during the course of this work. His great encouragement and support have helped me in all the time of this research. I am also deeply grateful to my graduate advisory committee, Dr. Dooyoung Hah and Dr. Ashok Srivastava for their valuable suggestions and support.

I am very thankful to Dr. Li Jiang for her precious suggestions. I am also deeply grateful to Mr. Golden Hwang for his countless technological help, and to Mr. James S. Breedlove for his exquisite handiwork to build many mechanical components. Lastly, I would like to express my special thanks to my parents, my brother and sister for their endless love and support.

TABLE OF CONTENTS

ACKNOWLEDGEMENTS....ii

LIST OF TABLES....v

LIST OF FIGURES....vi

ABSTRACT....viii

CHAPTER 1 INTRODUCTION....1
- 1.1 Background Terminology....1
- 1.2 Imprint Lithography....4
- 1.3 Accurate Alignment....6
- 1.4 Sources of Misalignment....9
- 1.5 Demolding Issues....10
- 1.6 Important Requirements for Imprint Stage....11
- 1.7 Research Objective....12

CHAPTER 2 THEORY....14
- 2.1 Beam Fixed at Both Ends....14
- 2.2 Euler's Limit....15
- 2.3 The Proposed Imprint Stage....16
- 2.4 Split Photodiode....18
- 2.5 Optical Magnification....22
- 2.6 Alignment Tracking Optics....22

CHAPTER 3 EXPERMENTAL DESIGN....26
- 3.1 Prototype Stage Construction and Set up....26
- 3.2 Optics for Detecting Stage's Vertical Position....29
- 3.3 Optics for Detecting Stage's Horizontal Position....31

CHAPTER 4 EXPERIMENTAL METHODS....34
- 4.1 Depth of Focus....34
- 4.2 Resonant Frequency....34
- 4.3 Vertical Stage Position vs. Horizontal Stage Position....35
- 4.4 Vertical Stiffness....36
- 4.5 Horizontal Stiffness....36

CHAPTER 5 RESULTS AND DISCUSSION....38
- 5.1 Depth of Focus....38
- 5.2 Resonant Frequency....38
- 5.3 Vertical Stage Position vs. Horizontal Stage Position....42
- 5.4 Vertical Stiffness....42
- 5.5 Horizontal Stiffness....45

CHAPTER 6 CONCLUSIONS 49

BIBLIOGRAPHY 51

VITA 52

LIST OF TABLES

5.1 Measurements of the vertical position of the stage and the time measurements of the video signal 43

5.2 Averaged one period, P, and analysis of time measurements data at every vertical position of the stage 43

5.3 Conversion of the time measurements to the stage's horizontal position..................44

5.4 Vertical displacements of the compressed & the uncompressed stage at different vertical force..46

5.5 Horizontal displacements of the compressed & the uncompressed stage at different horizontal force 48

LIST OF FIGURES

1.1 Numerical aperture of an optical system 3

1.2 Depth of focus of an optical system...3

1.3 Examples of three different imprint lithography (a) soft lithography
(b) nanoimprint lithography, NIL, (c) step and flash lithography, SFIL 7

1.4 Misalignment map showing mechanical shifts between the template
and substrate at contact 10

2.1 A long beam fixed at both ends (a) The vertical force, F_V,
displace the stage by a distance, D_V (b) The horizontal force, F_H,
displace it by a distance, D_H 14

2.2 A schematic figure of the practical stage which is stiff in all
horizontal directions. A second, perpendicular beam is added 14

2.3 Stage condition under different compressive loading ($F_B > F_{TH} > F_A$).
F_{TH} is the threshold force at Euler limit, $F_{TH} = (\pi^2 E h t^3)/12L^2$. (a) Below
Euler's limit (b) Above Euler's limit (c) At Euler's limit, $F_{ext} \approx 0$ 16

2.4 A proposed imprint stage with very high horizontal stiffness
(a) 3-D view, (b) side view. Compressive forces on the stage
reduce the vertical stiffness...17

2.5 Schematic plots of a photodiode current and voltage
vs. the stage vertical position 19

2.6 Schematics of the photodiode configurations 20

2.7 Schematics of the split photodiode current and voltage vs. the stage
vertical position, for each half of the split photodiode 21

2.8 The combined output voltage of the split photodiode vs.
the stage vertical position..21

2.9 The measured output voltage of the split photodiode vs.
The stage vertical position 21

2.10 Definition of optical magnification...22

2.11 Diffracted light beam by a diffraction grating 23

2.12 Optical system used to enhance the depth of focus of a grating (not to scale) Vertical fringes are formed where the ±1st order overlap 25

2.13 Depth of focus determined by the first orders of the incident light for different scales: (a) small scale showing a period of grating, p, (b) large scale showing the width of the beam, d, and the grating period, p 25

3.1 (a) A photo of experimental apparatus (b) A sketch of fundamental Experimental apparatus (not to scale) 27

3.2 Applied compressive force to the stage: (a) top view, (b) side view, (c) photograph 28

3.3 Optical system for detecting vertical position of the stage 29

3.4 A typical plot of the stage's vertical displacements vs. the photodiode voltages 30

3.5 Optical system for detecting horizontal position of the stage 31

3.6 In-focus fringe pattern on TV monitor..32

4.1 Typical averaged video signal, used to determine horizontal stage position.............35

5.1 Fringe patterns on the monitor over a stage's vertical motion of about 120 μm..39

5.2 Vertical stage oscillations (a) and (b), Vibrations observed with no compression on the stage. The scale of (a) are 10 msec/div in horizontal and 20 mV/div in vertical, and those of (b) are 1 sec/div in horizontal and 50 mV/div in vertical. (c) Stage compressed, increasing the peiod and decreasing the decay time of the oscillations. The horizontal scale is 100 msec/div, and the vertical scale is 20 mV/div..40

5.3 Change in horizontal position as the stage is moved vertically 44

5.4 Vertical displacements as a function of applied force in grams weight 46

5.5 Horizontal displacements as a function of applied force parallel to the stage in kilograms weight 48

ABSTRACT

The high-resolution capabilities of imprinting and step and flash lithography make these techniques strong contenders for the next generation lithography. Unfortunately, alignment remains an area of concern for nanoimprint because it must be completed before the template is moved into contact with the wafer. The large forces on the template during the process, even for step and flash, place additional demands on the stiffness as well as the reproducibility of the template stage. In this thesis, a prototype flexure stage has been developed to meet these demands. A compressive load, slightly below the Euler's limit, is used to produce relatively free motion in the vertical direction while maintaining extremely high horizontal stiffness. In addition, the horizontal stage position is viewed by an optical system based on a microscope objective with a central stop. With it the horizontal position of a diffraction grating fixed to the stage has been measured to a few nm, over a vertical range of several hundred microns. Consequently, not only does the high transverse stiffness of the stage minimize unwanted horizontal motions, but any that occur are measured over the entire required range of motion.

CHAPTER 1

INTRODUCTION

1.1 Background Terminology

1. Normal stress (σ): Stress, σ, is the applied force, F, on a material per unit area, A ($\sigma = F/A$). When the force is perpendicular to a cross-section area of the material, this stress is referred to normal stress.
2. Normal strain (ϵ): Strain is the geometrical deformation of the material under stress. Normal strain expresses a stretch without a shape change, and is the extended length, ΔL, of the material per its original length, L, ($\epsilon = \Delta L/L$).
3. Residual stresses: When a material is deformed by an applied external force, some stress may remain after removing the force. This stress is referred to as residual stresses.
4. Hooke's law: In the initial part of the stress-strain diagrams, the stress, σ, is directly proportional to the strain, ϵ ($\sigma = E\epsilon$). This relationship is referred as Hooke's law, where E represents Young's modulus. Young's modulus for steels are 190 ~ 210 GPa.
5. Stiffness (k): Stiffness is the ability of a material to resist a deformation under an applied force ($k = F/\Delta L$), where F represents the force and ΔL is the extended length.
6. Resonant Frequency: When a system oscillates with its maximum amplitude at a certain frequency, the frequency is referred to as the resonant frequency.

7. Numerical Aperture (NA): The numerical aperture of an optical system, NA, = $n\sin\theta$, where n is refraction index of the medium between the lens and the formed image, and θ is the half angle of the image forming cone (Figure 1.1).
8. Resolution (R): The minimum feature size that can be fabricated by a certain lithographic method. In optical lithography, resolution is limited by the wavelength of the light source and the optical system, and given by the equation, $R = K_1[\lambda / NA]$, where NA is the numerical aperture of the optical system, λ is the wavelength of the light used, and K_1 is a constant that includes all process related factors - its typical value is 0.5.
9. Depth of focus (DoF): When a lens forms an image, there is a range over which the image is in focus. This range is defined as the depth of focus as shown in Figure 1.2. DoF is defined such that the blur circle is twice the resolution, and governed by the equation, $DoF = K_2 [\lambda / NA^2]$, in optical lithography, where NA is the numerical aperture of the optical system, λ represents the wavelength of the light, and K_2 is a constant for a specific lithographical process.
10. Critical Dimension, CD: The minimum width line or space in a properly operating device.
11. Overlay control: Layer to layer alignment throughout a device during multilayered device fabrication. The importance of accurate overlay control has grown larger as more advanced technology produces smaller and more highly packed chips. The required overlay accuracy is about one third of the minimum feature width.

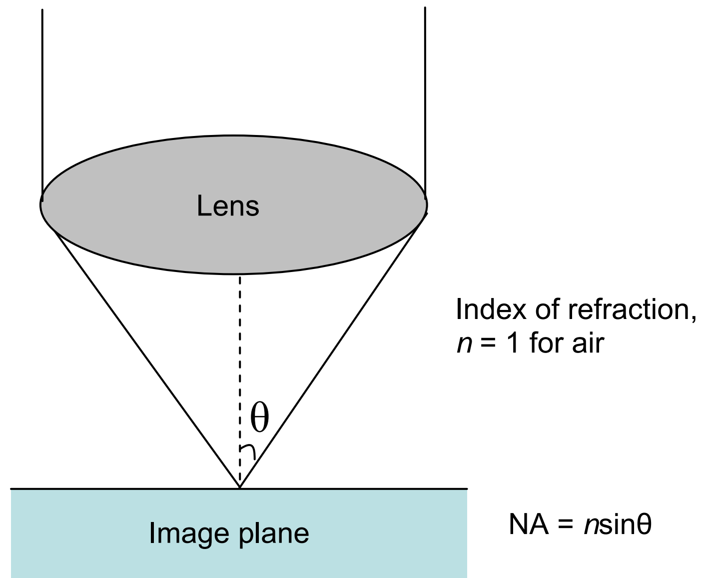

Figure 1.1 Numerical aperture of an optical system.

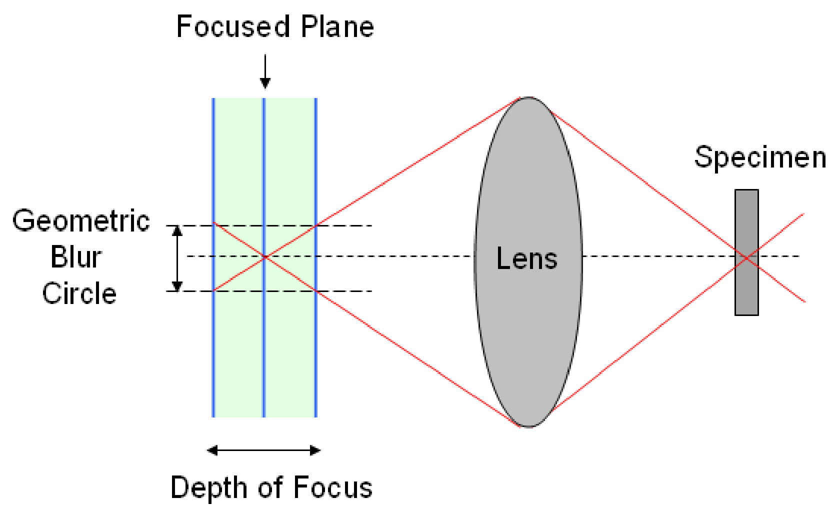

Figure 1.2 Depth of focus of an optical system.

1.2 Imprint Lithography

Optical lithography has been employed as a conventional pattern transferring method in the integrated circuit industry and greatly improved over the last few decades following Moore’s law. These improvements have been achieved in the past by reducing the wavelength of the light source, by increasing the numerical aperture of the lens, and by optical enhancements such as phase shift masks and oblique illumination. In addition, immersion lithography, which employs a liquid medium between the lens and wafer to increase the numerical aperture of the system, has also emerged with enhanced resolution, below 50 nm. However, optical lithography is reaching a limit due to physical limitations as well as the significant cost of the optical systems.

As conventional lithography reaches its limit, several alternative methods such as electron beam lithography, focused ion beam lithography, and scanning probe lithography have demonstrated better resolution. These methods overcome the diffraction limit of optical lithography by directly writing a pattern on a wafer with high energy beams or a mechanical probe. However, the writing time with these lithographies is too long to replace conventional optical lithography for high level mass production.

Imprint lithography, a promising candidate for the next generation lithography, has attracted great attention due to its superior resolution, high throughput, and low cost. Imprint lithography is a micro/nanomolding process which transfers patterns on a stamp or template to a resist on a substrate by pressure. The stamps are usually fabricated with conventional electron beam or focused ion lithography, and they can be used to replicate the patterns many times with excellent resolution and high throughput. Not only does imprint lithography not require an expensive optical system, it has also been

demonstrated that this technology can decrease the minimum feature size down to the 10 nm region. However, there are still several concerns that need to be resolved, for example, stamp fabrication, polymer issues, residual layer control, process control, accurate alignment, developing suitable tools, and system automation. Of these, alignment is probably the most critical, particularly for developing smaller transistors that require multiple process levels.

Various imprinting techniques have been demonstrated in an effort to decrease the minimum feature size. There are three main approaches[1]: soft lithography, nanoimprint lithography (NIL), and step and flash imprint lithography (SFIL). Soft lithography is a process of fabricating or replicating structures by using elastic stamps. The elastic stamps are typically fabricated by pouring PDMS (Polydimethylsiloxane) prepolymer to a master that was fabricated by a conventional lithography technique, and then peeling the PDMS off the master after the curing process. The resulting elastic PDMS stamps have been used in various soft lithographic processes such as micro-contact printing (μCP), micro-replica molding (REM), micro-transfer molding (μTM), micromolding in capillaries (MIMIC), and solvent-assisted micromolding (SAMIM). Of these, micro-contact printing technique is the most popular, and a basic fabrication sequence is shown in Figure 1.3(a). The PDMS stamp is inked with a self-assembly layer before the soft imprint. After the stamp is removed, the transferred self-assembly layer is used as an etch barrier for the further process. Although soft lithography is a convenient, effective, and low cost method, the applications are limited to biotechnology and plastic electronics because the PDMS is easily deformable. Therefore, a more precise method is necessary to fabricate multilayer devices or large devices with small features.

Nanoimprint lithography (NIL), developed by Chou et al., uses a rigid mold, typically silicon or nickel (Figure 1.3(b)). The resist on the substrate is heated above its glass transition temperature, and the mold is pressed upon it with a relatively large force to transfer patterns. Next, the substrate is cooled, the pattern on the resist solidifies, and then the mold is removed. This patterned resist layer is used as an etch barrier for further processing. Although nanoimprint lithography has demonstrated resolution down to 10 nm, overlay issues are very challenging for applying this technique to fabricate multilayer devices. The high temperature and pressure during the imprint process exacerbate the overlay errors.

Step and flash lithography (SFIL), developed by Colburn et al., uses a transparent rigid template such as quartz to minimize the overlay issues of nanoimprint lithography (Figure 1.3(c)). A low viscosity resist is locally applied on a substrate, and then the template is brought into contact with the resist layer. Ultra violet (UV) light is applied through the transparent template onto the resist layer to cure and solidify it at room temperature. Adopting UV curable resist has two significant advantages over NIL; unlike NIL, it does not require either high temperature or high pressure, which are the key sources of error for multilayer overlay.

1.3 Accurate Alignment

Nanoimprint and step and flash lithography have demonstrated resolutions in the 10 nm range, making them strong contenders for the next generation lithography. In addition, this technology can be used in various areas besides integrated circuits: MEMS, optical devices, and other nanodevices. For most applications to be successful, alignment must be very accurate, because most of these devices have multiple layers to perform

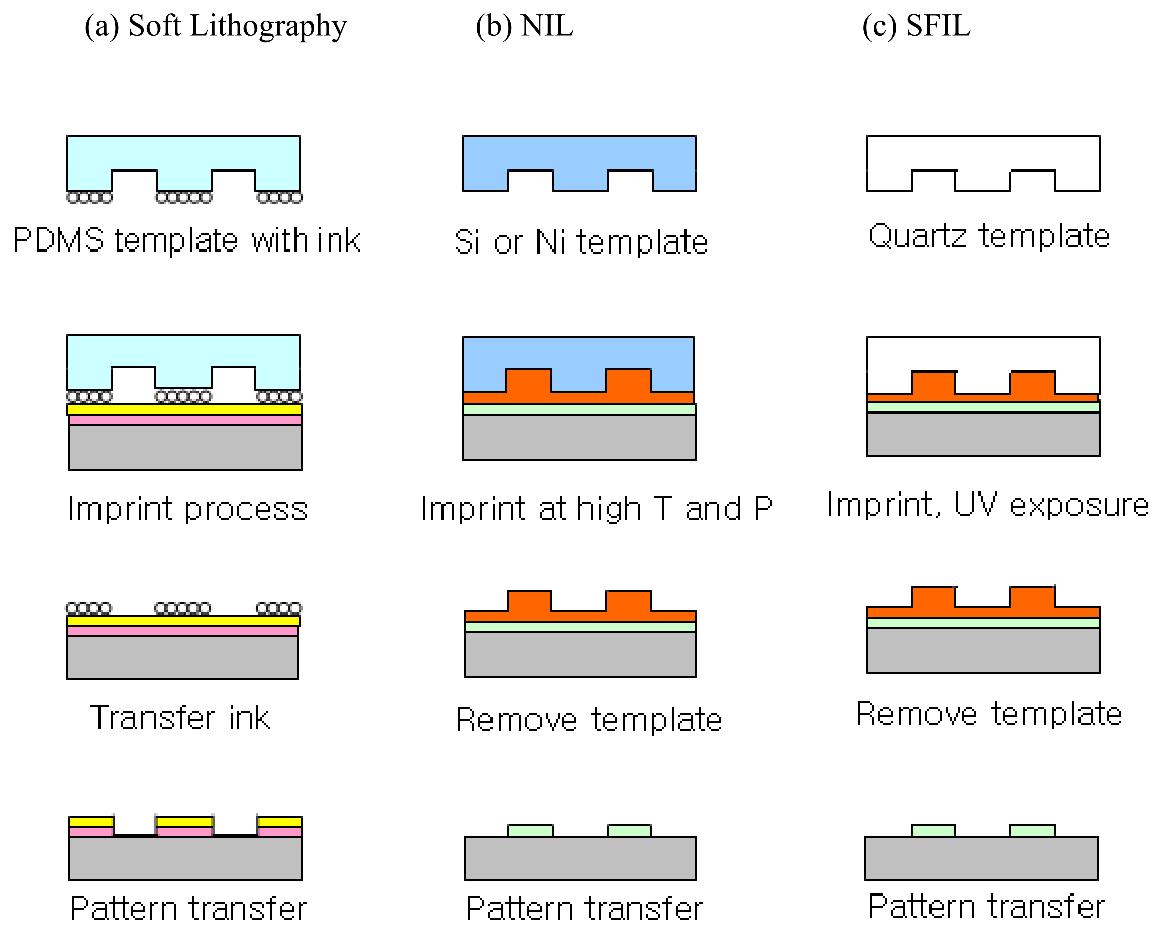

Figure 1.3 Examples of three different imprint lithography (a) soft lithography (b) nanoimprint lithography, NIL, (c) step and flash lithography, SFIL [redrawn from ref.1].

their complex functions. However, alignment still remains an area of concern for imprinting because it must be completed before the template is moved into contact with the wafer. The large forces on the template during the process, even for step and flash, place additional demands on the stiffness as well as the reproducibility of the template stage.

While nanoimprint lithographic tools have not yet conquered accurate alignment difficulties, some step and flash lithographic tools have been demonstrated with new alignment techniques by modifying commercial optical aligners, for example, by replacing the mask holder with the template stage.[2-4] However, their best resulting alignment accuracy was limited to the submicron range.[2] Molecular imprints, Inc (MII), one of the leading companies for developing nanolithography tools, has commercialized step and flash nanoimprint tools. The company states that Imprio 100, the first step and flash nanoimprint system, has sub-50 nm resolution and sub-500 nm 3σ alignment accuracy and that Imprio 250, which they called as "the industry's most advanced imprint lithography system," has sub-50 nm resolution and sub 10 nm 3σ alignment accuracy.[5] Although this considerable improvement is impressive, their applications are limited to small scale manufacturing facilities, and their tools are essentially designed to target areas such as compound semiconductor development, photonics, MEMS, molecular electronics, etc., rather than the silicon IC industry. Besides, NIL has demonstrated worse alignment results than SFIL because of the magnification and distortion errors caused by high temperature and pressure during process. Unfortunately, the overlay required, about one third of the minimum feature width in integrated circuits, has yet to be demonstrated. Therefore, further research is required to develop more reliable imprint tools with better

resolution, higher throughput, and especially more accurate alignment capability.

1.4 Sources of Misalignment

Zang and Chou[6] reported several sources of misalignment in imprint lithography. One important factor is mechanical shifts and rotations between the template and the substrate during the imprinting process. Figure 1.4 illustrates a misalignment map showing mechanical shifts during the imprint process.[6] Two main factors of the misalignment are considered. First, the template and substrate holders may bend during the imprint process because they are not precisely parallel to each other. Second, the pressure applied at contact is often non-uniformly distributed resulting in unwanted displacements since their surfaces are not exactly flat. Therefore, it is important to develop an imprint machine that is capable of eliminating the mechanical shifts between the template and substrate and of dynamically aligning them during the imprint process.

The difference in thermal expansion coefficient between the template and substrate is another important source of misalignment, especially when the two plates are of different materials. This factor is particularly severe for nanoimprint lithography because it involves a high temperature during the imprint process after alignment at room temperature. However, this issue should be also considered for step and flash lithography since the template and substrate are also heated during the UV curing step.

Any temperature non-uniformity over the resist on the substrate may also cause misalignment in imprint lithography. In addition to thermal distortions, temperature is a key factor in the resist viscosity and the resist filling time; it must be carefully controlled and evenly distributed over a wafer to perform accurate alignment. Resists with lower glass transition temperatures could enhance alignment uniformity since lower imprint

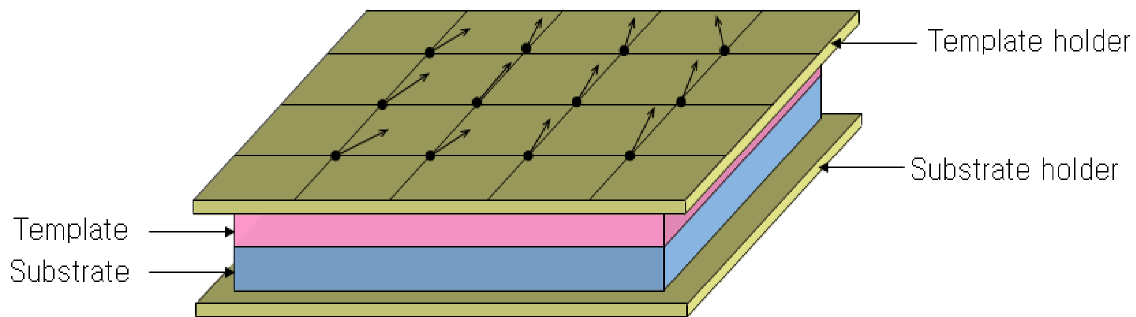

Figure 1.4 Misalignment map showing mechanical shifts between the template and substrate at contact [redrawn from ref. 6].

temperature usually implies better temperature uniformity control during the imprint.

1.5 Demolding Issues

Many imprint failures occur during the demolding step. In this respect, the demolding force must be carefully controlled, and imprint tools must be developed to meet these demands. Demolding force depends on various factors: stamp geometries, chemistry, and the demolding temperature. For example, templates with higher aspect ratio patterns require higher demolding forces, and the force may change when different stamp materials and resists are used. An anti-adhesion layer is usually applied between the template and the substrate to reduce friction and the demolding force between them. However, the effect of temperature on demolding is not yet completely understood. Using a higher demolding temperature can be more successful when there is a strong adhesion between the template and resist; however, the lower temperature can be better when a highly efficient anti-adhesion layer is applied between the template and the resist.

Another important consideration during the demolding process is that the template stage must be moved vertically from the template surface, back to its original position. If the template motion slants from the vertical, the demolding force and stresses increase, and the transferred patterns can be easily destroyed. Therefore, imprint tools capable of moving vertically during both imprint and demolding steps (i.e., highly reproducible imprint tools) are necessary to increase both the yield and overlay accuracy. The template stage motion must be reproducible, to the nanometer level, even in the presence of large sideways forces at contact.

1.6 Important Requirements for Imprint Stage

Previous work[7] demonstrated a reproducible cantilever stage as an imprint lithography tool with alignment optics. The fundamental concept of the idea is to align the template and wafer when they are separated by a small gap, and then bring the template into contact with the wafer. There are three important conditions for the imprint stage: First, the alignment optics must form high resolution images of the template and the wafer when they are separated by a large gap. It is desirable, although not necessary, that the alignment optics have a depth of focus large enough for the image to remain in focus throughout the imprint process. Second, the template must be brought into contact with wafer over the gap preferably without any shifts or changes in overlay, and this procedure should be monitored. Finally, the template stage must be separated from the wafer in a purely vertical motion, in spite of any large sideways forces that may exist at contact. In other words, the stage should have high horizontal stiffness as well as reproducible motion.

1.7 Research Objective

This thesis developed a new prototype stage which is suitable for imprint lithography. After constructing the stage based on the previous work and theory, the stage's properties were studied both experimentally and analytically. It was shown that the stage moves relatively freely in the vertical direction, but is extremely stiff horizontally. In addition, an optical system capable of continuously tracking any unwanted horizontal stage motions as the stage moved over a large vertical distance was demonstrated. The research consisted of the following subtasks.

1. Stage setup: The prototype stage was constructed and set up to be freely moving in the vertical direction but to be extremely stiff horizontally. It was demonstrated that compressive loading applied to the stage meets this condition.
2. Optical system constructions: Optical systems were constructed to display the vertical and horizontal motions of the stage.
3. Vertical stage oscillations: The resonant frequencies of both the compressed and the uncompressed stages were measured.
4. Calibration of the stage's vertical displacements: The vertical position of the stage was calibrated with a digital caliper.
5. Relation between the horizontal and the vertical stage's positions: Horizontal stage motions were measured over the entire required range of vertical motion, and then analyzed.

6. Measurements of the vertical stage displacements: The vertical stage compliance was measured by applying vertical forces to both the compressed and the uncompressed stages. The vertical stiffness was studied.
7. Measurements of the horizontal stage displacements: The horizontal stage compliance was measured by applying horizontal forces to both the compressed and the uncompressed stages. The horizontal stiffness was studied.

CHAPTER 2

THEORY

2.1 Beam Fixed at Both Ends

The prototype imprint stage is based on a long beam that is fixed at both ends. As shown in Figure 2.1, the application of a vertical force, F_V, at the center, displaces the stage vertically by a distance, D_V, and the vertical spring constant, K_V, is defined by $F_V = K_V D_V$. Similarly, the horizontal spring constant K_H, is defined by $F_H = K_H D_H$, where F_H and D_H are a horizontal force parallel to the long direction of the stage and the resulting deflection. It is desirable for the stage to be much stiffer in the horizontal direction than in the vertical direction, i.e., $K_H >> K_V$. In addition, a practical stage must be stiff in all horizontal directions, which can be achieved by adding a second, perpendicular beam (Figure 2.2).

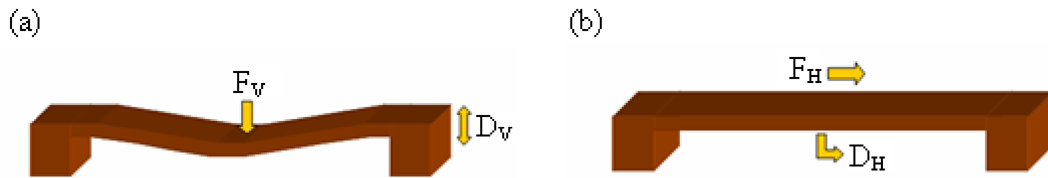

Figure 2.1 A long beam fixed at both ends. (a) The vertical force, F_V, displaces the stage by a distance, D_V (b) The horizontal force, F_H, displaces it by a distance, D_H.

Figure 2.2 A schematic figure of the practical stage which is stiff in all horizontal directions. A second, perpendicular beam is added.

2.2 Euler's Limit

When a compressive force, F, is applied to a long beam fixed at both ends, a stress, $\sigma = F/A$, is created, where A is the cross sectional area of the beam. As shown in Figure 2.3, if the applied force, F, is smaller than the threshold force, F_{TH}, the beam will remain straight; however, if F is greater than F_{TH}, it will be unstable, snapping into a deflected state either above or below the median plane. The critical load or threshold force, F_{TH}, at which this occurs is called the Euler's limit, given by

$$F_{TH} = \frac{\pi^2 \mathrm{E}\, ht^3}{12L^2} \tag{2.1}$$

where h, t, and L are the height, thickness, and length of the beam respectively, and E is its Young's modulus. At the Euler's limit the vertical spring constant, K_V, approaches zero; i.e., the stage becomes completely compliant vertically. Since the horizontal stiffness is relatively unaffected, this property may be exploited to make a stage that moves freely in the vertical direction, but is extremely stiff horizontally.

In theory at the Euler's limit $K_V = 0$ only when $D_V = 0$. In practice near the Euler limit there is a substantial range of D_V where K_V is small and approximately constant. The variation in K_V near the Euler's limit is readily observed by measuring the frequency, f, of vertical oscillation of the stage:

$$f = \frac{1}{2\pi}\sqrt{\frac{K_V}{m}} \tag{2.2}$$

where m is the effective mass of the stage. Once excited the oscillations are nearly sinusoidal, decaying exponentially because of internal friction in the stage material.

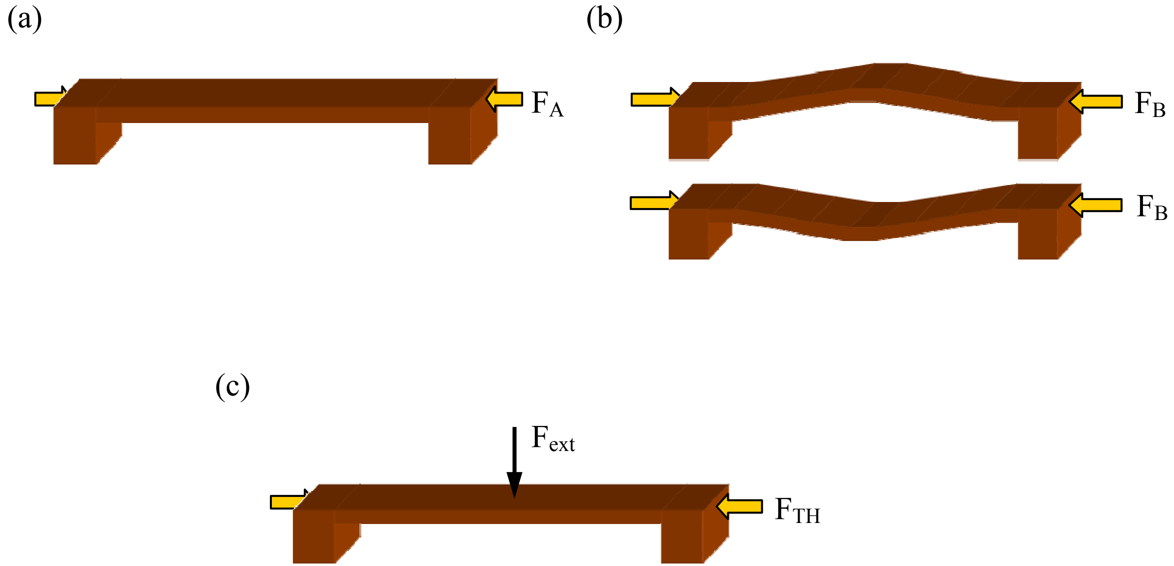

Figure 2.3 Stage condition under different compressive loading ($F_B > F_{TH} > F_A$). F_{TH} is the threshold force at Euler limit, $F_{TH} = (\pi^2 E h t^3)/12L^2$. (a) Below Euler's limit (b) Above Euler's limit (c) At Euler's limit, $F_{ext} \approx 0$.

2.3 The Proposed Imprint Stage

The proposed stage in this thesis satisfies the important requirements for the ideal imprint stage discussed in Section 1.7. This imprint stage is based on the two beams joined at right angles providing high stiffness in all horizontal direction (Figure 2.4). In addition, a compressive load, F, slightly below the Euler's limit, is used to produce relatively free motion in the vertical direction while maintaining most of the extremely high horizontal stiffness. Any shifts in the horizontal directions will be minimized during the vertical motion due to the high stiffness of the stage.

The flat template stage is loaded at the joint place, and the wafer stage is positioned just below it separated by a small gap. The vertical stage motion has reliable

vertical reproducibility over multiple imprint process. For example, a magnetic coil can be used to drive the stage motion, and the multiple stage travels were demonstrated in previous work.[7]

Alignment can be completed before the template stage is moved into contact with the wafer by adopting high resolution optics based on a microscope objective. Not only imaging both the template and substrate patterns at the gap, but it is also capable of imaging them throughout the imprint process due to large depth of focus. In addition, the real vertical position of the stage is measured by adopting another optical system based on a split photodiode. These optical systems can verify the true motion of the stage and detect any unwanted horizontal displacement over the entire range of the vertical movement. Any alignment errors can be detected and corrected during the process resulting in reduction in the alignment errors.

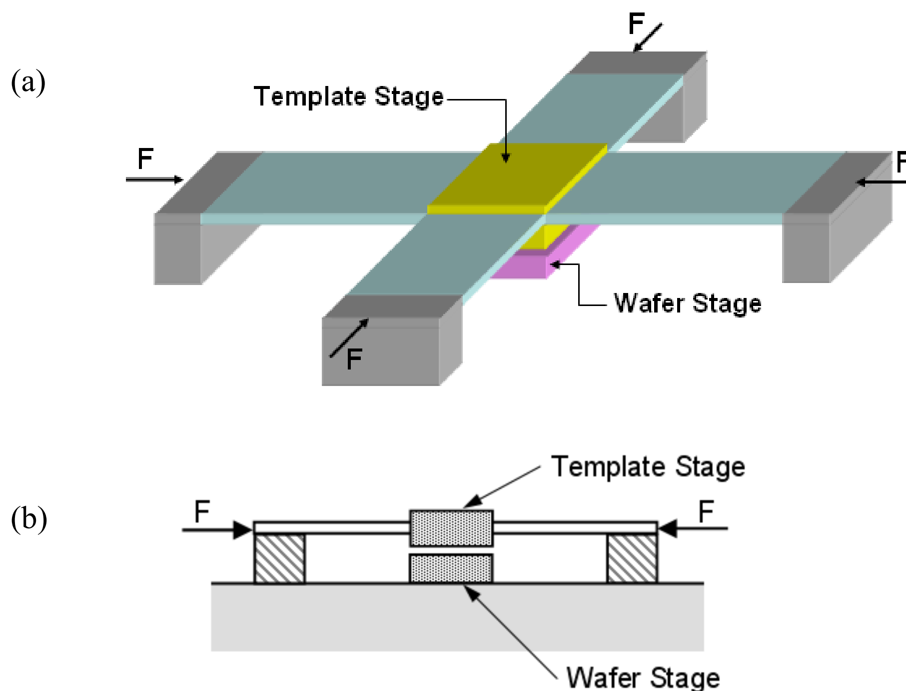

Figure 2.4 A proposed imprint stage with very high horizontal stiffness (a) 3-D view, (b) side view. Compressive forces on the stage reduce the vertical stiffness.

2.4 Split Photodiode

Photodiodes are semiconductor devices that detect optical signals and convert the optical signals into electrical signals. Photodiodes may have a p-n junction or p-i-n junction structure. When a photon with a sufficient energy (larger than the bandgap energy, $h\upsilon > E_g$) is absorbed by a photodiode, an electron-hole pair (EHP) is created. If this carrier generation occurs in either the depletion region or within the diffusion length from it, the electrons and holes are swept from the junction by a potential, generating a current, a voltage, or both. The potential results from the contact potential plus any external applied voltage.

The photodiode is usually operated under either zero current (photovoltaic mode) or reverse bias (photoconductive mode). In the photovoltaic mode, when light falls on the junction, a forward voltage is produced across the device. This conversion is called the photovoltaic effect. The photodiode also can be operated under reverse bias, and this induces a small saturation current. The basic operation in the reverse bias mode is similar to that of the photovoltaic mode; however, the increased depletion layer formed by the reverse bias improves its performance, for example, it is more sensitive to light and has lower capacitance, decreasing its time response.

In this thesis, a photodiode is used to detect the vertical position of the test stage. The basic concept is that the light source is reflected from a mirror on the stage to a photodiode, and the output photodiode voltage is measured. As the stage moves vertically, the reflected light sweeps across the photodiode, resulting in varying the output voltage. Figure 2.5 shows schematic plots of a photodiode current and voltage as a function of the stage's vertical position under the assumption that the incident laser is a

uniform square beam, and the size of the laser beam is equal to that of the photodetector. The highest voltage is achieved when the incident light is centered on the photodiode. As the stage moves either upward or downward, the light on the diode reduces, resulting in a symmetrical decrease in the output current and voltage. Note that the photodiode current is proportional to the incident light amount and has a logarithmic relationship with the voltage. The current, I, is given by

$$I = I_0 \, e^{V/KT} \tag{2.3}$$

where I_o is the saturation current, V is the voltage across the diode, K is the Boltzman constant, and T is temperature. The voltage is given by

$$V = KT \, ln \frac{I}{I_0} \tag{2.4}$$

There is not a linear relationship between the output voltage and the position of the stage.

This work used a split photodiode (Figure 2.6) with the two halves wired in series opposition. Each photodiode voltage of the split photodiode has a logarithmic relationship with the current, given by

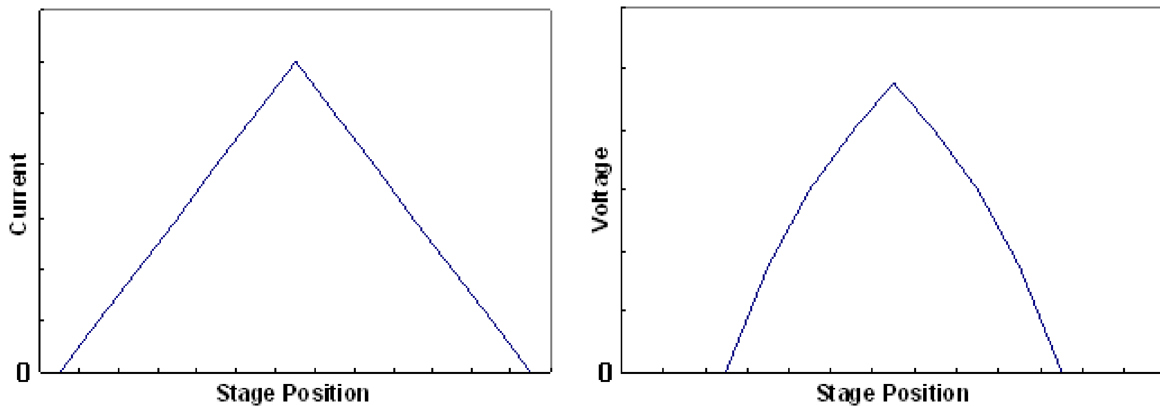

Figure 2.5 Schematic plots of a photodiode current and voltage vs. the stage vertical position.

$$V_L = KT\, ln\frac{I_L}{I_0}$$

$$V_R = KT\, ln\frac{I_R}{I_0} \tag{2.5}$$

where V_L and I_L are voltage and current of the left photodiode; likewise, V_R and I_R are those of the right photodiode. Therefore, the combined output voltage across the split photodiode has the following relationship.

$$V_L - V_R = KT\left(ln\frac{I_L}{I_0} - ln\frac{I_R}{I_0} \right) = KT\, ln\frac{I_L}{I_R} \tag{2.6}$$

Figure 2.7 shows sketches of the current and voltage of the two diodes, left and right, in the split photodiode as a function of the stage vertical position under the same assumptions. This configuration improves the linearity between the voltage and the stage position, because the outputs of the split photodiode oppose each other (Figure 2.8). In addition, it also extends the vertical measurement range by adding the two output voltages. The curvature of the first photodiode voltage is largely offset by the second photodiode output. In addition, when the stage is positioned at the median plane, the combined output voltage is zero. Figure 2.9 is a plot of the measured voltage of the split photodiode as a function of the vertical position of the stage, and shows a good agreement with the theory.

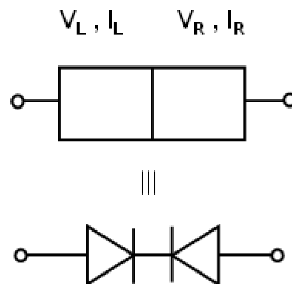

Figure 2.6 Schematics of the photodiode configurations.

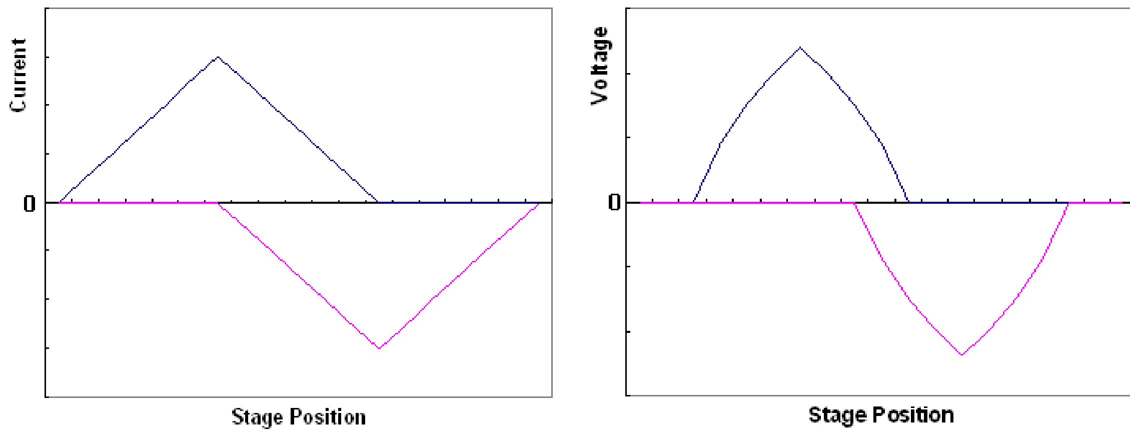

Figure 2.7 Schematics of the split photodiode current and voltage vs. the stage vertical position, for each half of the split photodiode.

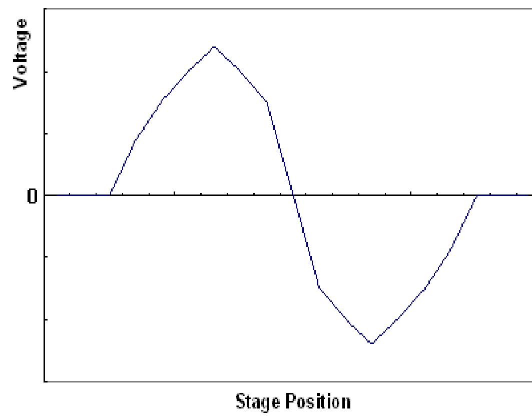

Figure 2.8 The combined output voltage of the split photodiode vs. the stage vertical position.

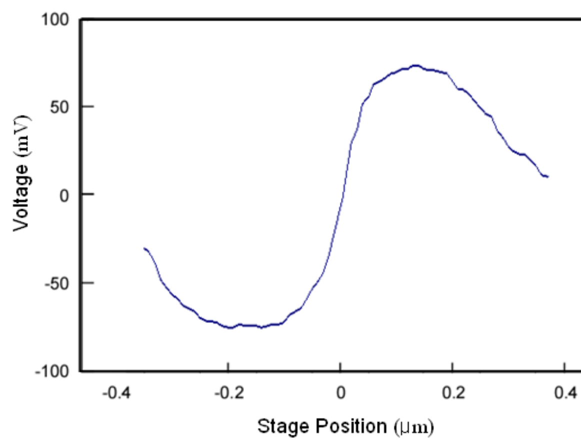

Figure 2.9 The measured output voltage of the split photodiode vs. the stage vertical position.

2.5 Optical Magnification

Optical magnification is defined as the ratio between the size of an object and its image (Figure 2.9). For a single lens,

$$Magnification \equiv \frac{y_2}{y_1} = \frac{s_2}{s_1} \tag{2.7}$$

where y_1 is the original size of an object, y_2 is its image size, s_1 is the distance between the object and lens, and s_2 is the distance between the lens and the image. For a high power microscope objective, $s_1 \approx$ its focal length.

2.6 Alignment Tracking Optics

A grating of period P diffracts a parallel, coherent light beam, e.g., a laser beam, into several orders (Figure 2.10). A lens, e.g., a microscope objective, may then form a magnified image of the grating, with greater or lesser fidelity depending on how many diffraction orders pass through it. Of particular interest is the case where the zero order is blocked, e.g., by a stop inserted into the lens, and the numerical aperture of the lens limits the diffracted light to only the $\pm 1^{st}$ orders (Figure 2.11).

Previous work in our laboratory has demonstrated that the depth of focus is greatly extended in this case.[8] The large depth of focus is essential for the alignment

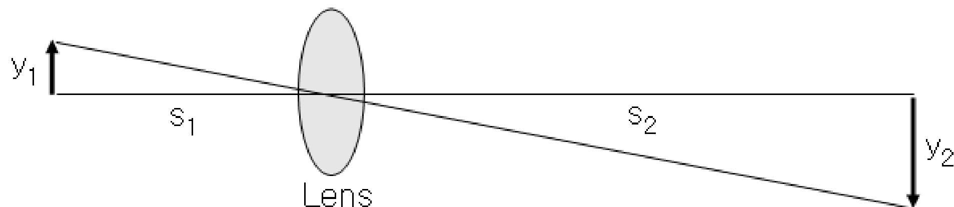

Figure 2.10 Definition of optical magnification.

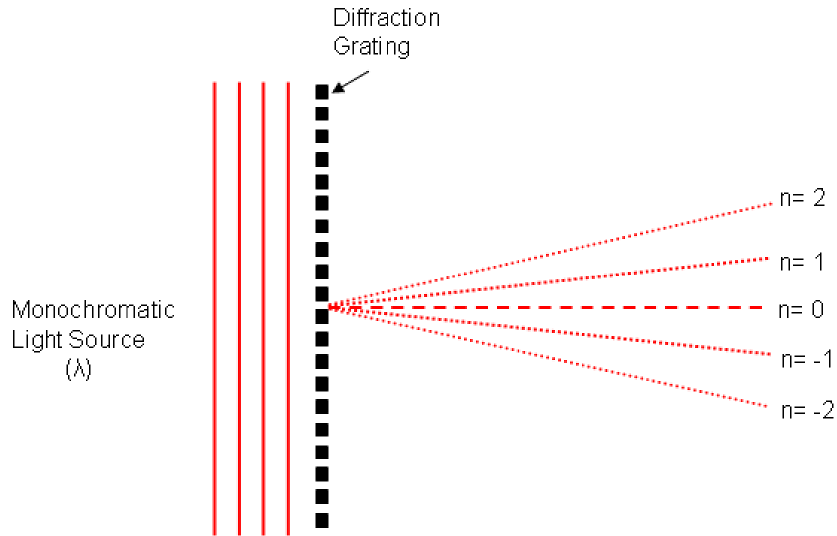

Figure 2.11 Diffracted light beam by a diffraction grating.

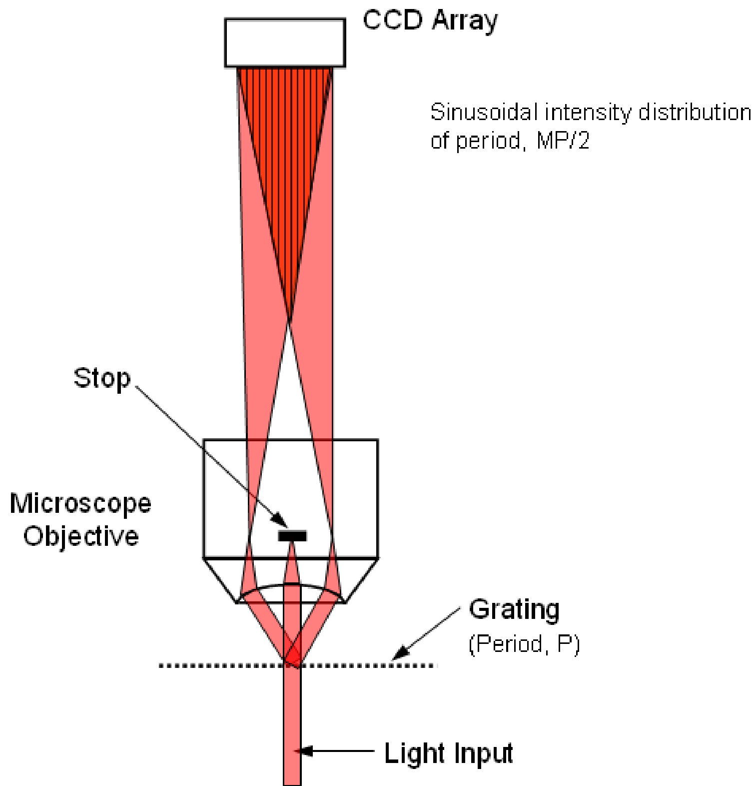

Figure 2.12 Optical system used to enhance the depth of focus of a grating (not to scale). Vertical fringes are formed where the $\pm 1^{st}$ order overlap.

process particularly when topography of template and wafer is involved. In addition, it is also necessary to form sharp images of both a template and a wafer throughout the imprint process.

If the magnification of the lens is M, then the image of the grating (period, P) has a sinusoidal intensity distribution of period MP/2.[8] The separation between the lens and the grating is not critical; the depth of focus is determined by the overlap of the $\pm 1^{st}$ orders and is comparable to the width of the incident light beam. It is given by

$$DoF = \frac{d}{\tan\theta}$$

(2.8)

where d is the width of the laser beam, and θ is the incident light angle as shown in Figure 2.12.

The depth of focus of the optical system can be theoretically calculated with the above equation. As can be seen in Figure 2.12, the n'th order beams are diffracted at an angle, θ, given by

$$p\sin\theta = n\lambda \tag{2.9}$$

where p is the grating period, λ is the wavelength of the incident light, and n represents the diffraction order. For λ = 633 nm, p = 2 μm, and n = 1

$$\sin\theta = \frac{n\lambda}{p} = \frac{1\times 633}{2000} = 0.3165$$

$$\theta = 18.45^{\circ} \tag{2.10}$$

$$DoF = \frac{d}{\tan\theta} = \frac{1}{\tan(18.45)} \approx 3.00 \tag{2.11}$$

Therefore, the depth of focus is about 3 mm, for d = 1 mm, and θ = 18.45°.

(a)

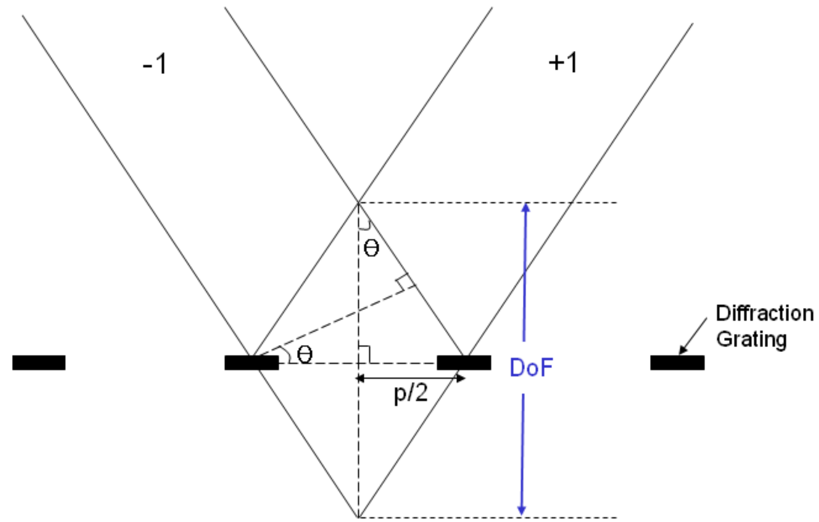

(b)

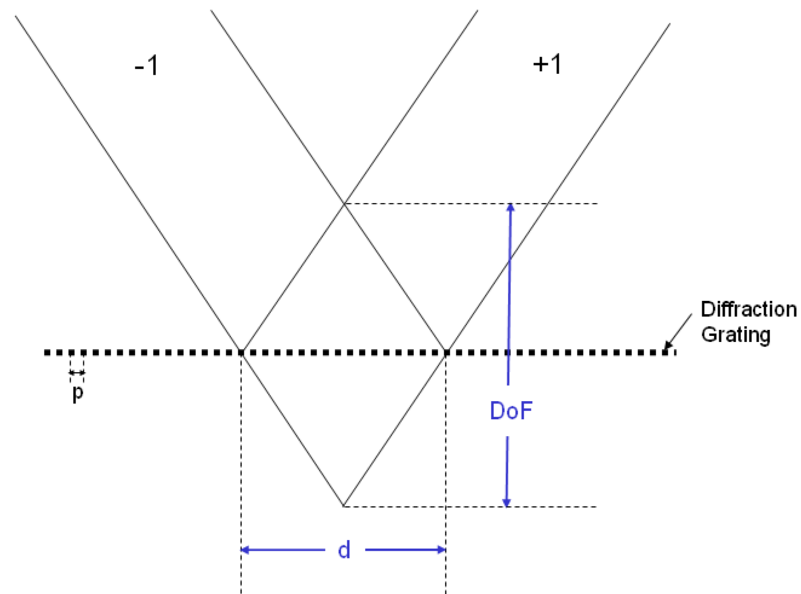

Figure 2.12 Depth of focus determined by the first orders of the incident light for different scales: (a) small scale showing a period of the grating, p, (b) large scale showing the width of the beam, d, and the grating period, p.

CHAPTER 3

EXPERIMENTAL DESIGN

3.1 Prototype Stage Construction

Figure 3.1 shows the basic experiment apparatus. The test stage was based on a steel bar, 5 cm wide by 3 mm thick and 60 cm long. The stage was bolted at each end to an optical table and kept in a horizontal plane by adjusting the bolts on the right hand side around a fulcrum. In addition, a 2 μm period transmission diffraction grating was fixed to the stage. The optical systems were set up to study the vertical and horizontal motions of the test stage. A more detailed description of the optics is in the following Sections 3.2 and 3.3.

Compressive loading on the stage was produced by a lever and push-rod mechanism at one end (Figure 3.2). The axial loading was controlled by tightening or loosening the screw D. While the support was rigidly fixed to the optical table with the two of the screws C, only the top of the lever arm was pinned. A link located between the lever arm and the right hand side of the stage transmitted the force to the stage. Therefore, tightening the screw D increased compressive force on the stage, and loosening the screw reduced the force. In practice, the compressive load was set at slightly below the Euler's limit, where the resonant frequency was minimized before the stage became unstable (more details in Section 3.4).

The test stage was set straight and level by adjusting the screws A and B at the right hand side before every experiment. The screws were adjusted to maintain the center of the stage at its median height as the compression was applied. For example, tightening

screws A and loosening screws B resulted in pushing down the stage; loosening screws A and tightening screws B pulled the stage up.

(a)

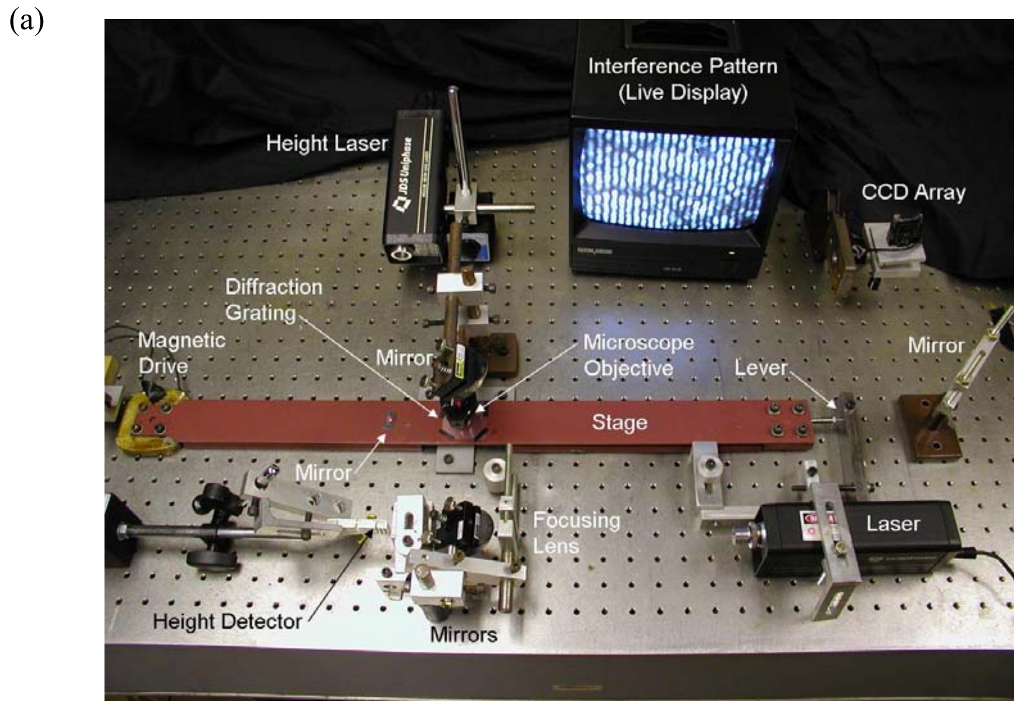

(b)

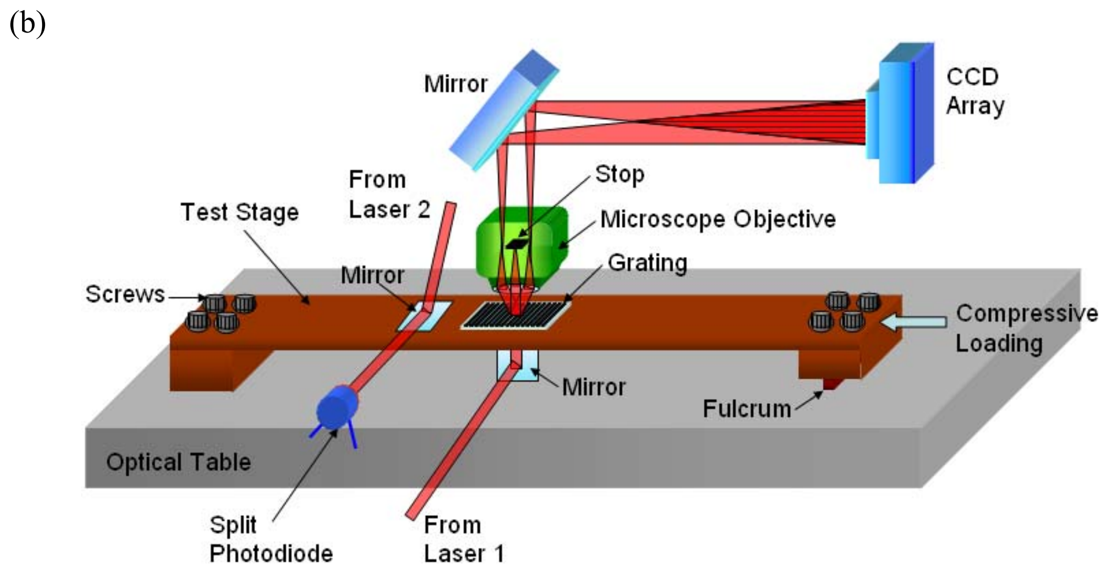

Figure 3.1 (a) A photo of experimental apparatus (b) A sketch of fundamental experimental apparatus (not to scale).

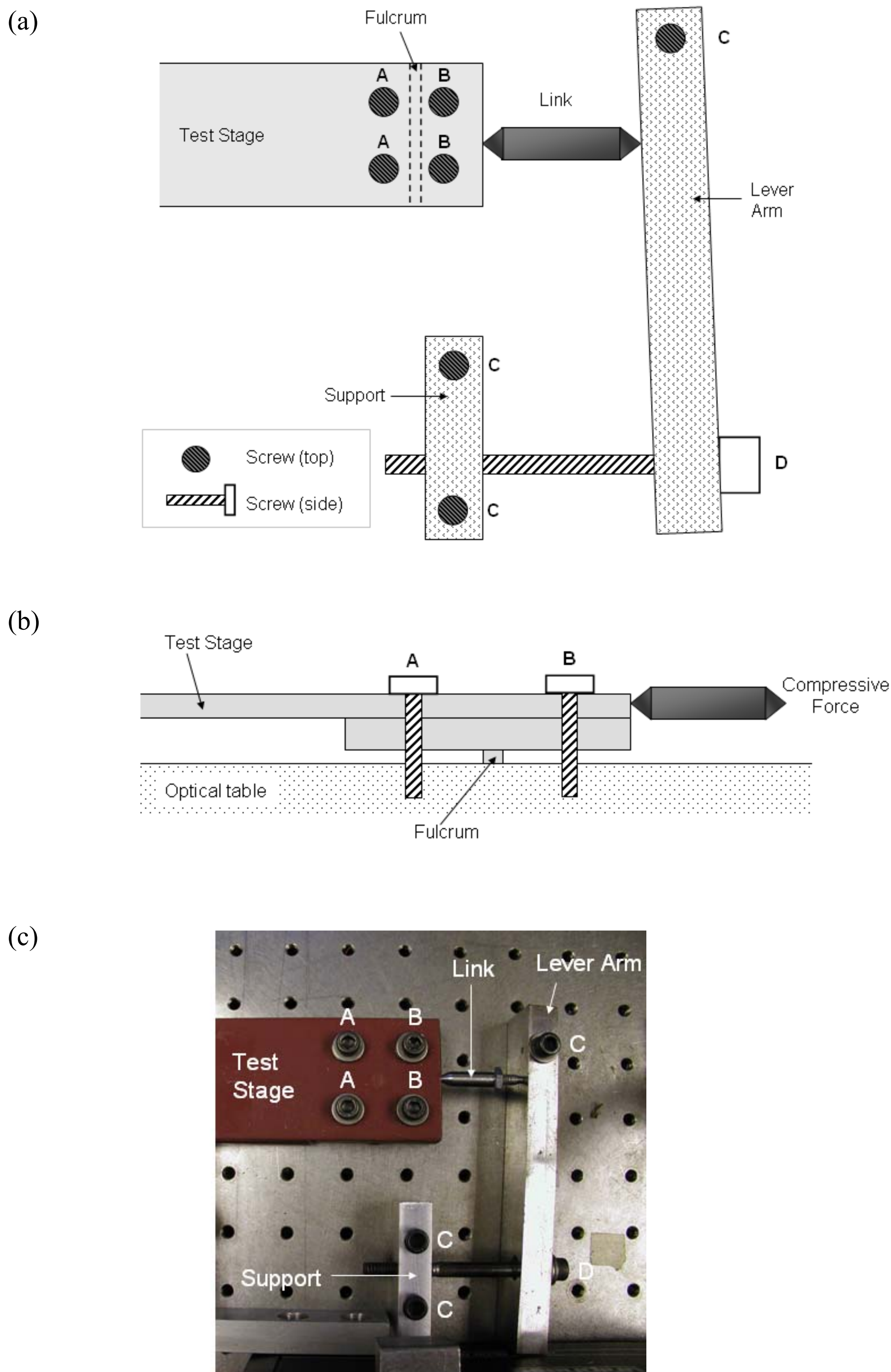

Figure 3.2 Applied compressive force to the stage: (a) top view, (b) side view, (c) photograph.

3.2 Optics for Detecting Stage's Vertical Position

The height of the stage was monitored by reflecting a HeNe laser beam at 633 nm from a mirror to a split photodiode as shown in Figure 3.1, and in more detail in Figure 3.3. The laser beam was reflected at a grazing angle from a mirror near the center of the stage onto a split photodiode. The two halves of the split photodiode were connected in the photovoltaic mode in series opposition, and their combined output was read with a digital voltmeter and a digital storage oscilloscope.[9]

The photodiode was initially positioned so that the combined output voltage was zero when the stage was straight and level. Next, the stage height was slightly varied by adding weights on the stage or pulling it up with a spring. At the same time, the photodiode voltages were measured, and the displacements were calibrated with a digital caliper.[10] A plot of the vertical displacements as a function of the the split photodiode voltages was drawn in Figure 3.4, and was nearly linear over a range of 120 μm. This plot has been used to determine the vertical positions of the stage by measuring the photodiode voltages throughout this research.

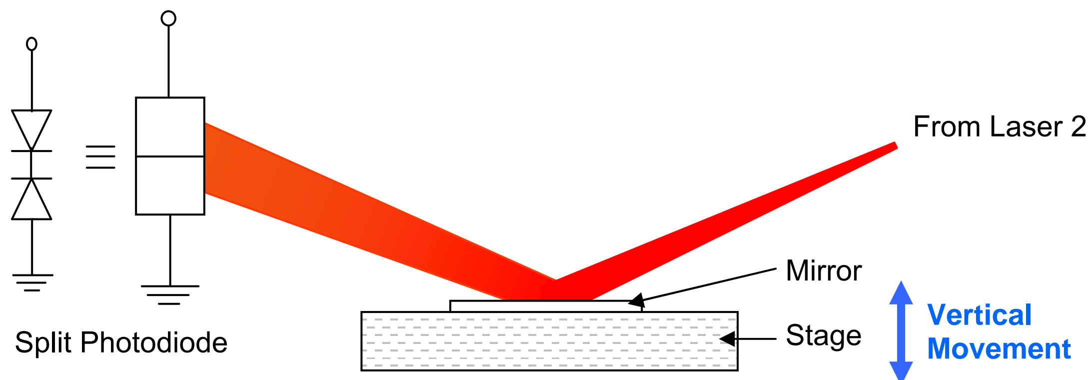

Figure 3.3 Optical system for detecting vertical position of the stage (not to scale).

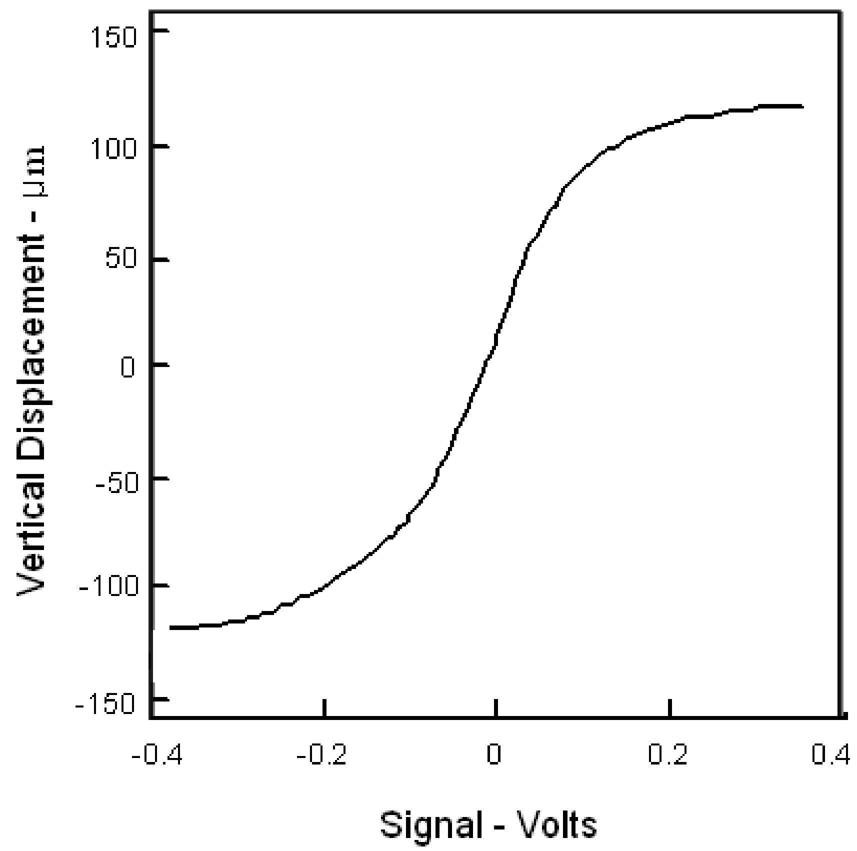

Figure 3.4 A typical plot of the stage's vertical displacements vs. the photodiode voltages.

3.3 Optics for Detecting Stage's Horizontal Position

The horizontal position of the stage was monitored by passing a second HeNe laser beam at 633 nm through a 2 μm period grating fixed to the stage as shown in Figure 3.1 and in more detail in Figure 3.5. First, the laser beam was reflected by a mirror underneath the stage through a small hole in the center of the stage, and then diffracted by the grating into three beams, i.e., 0, +1, and -1 orders. The two first-order beams passed through a 43X, 0.65 NA microscope objective, but the zero-order beam was blocked by adding a stop, a dot in the center of a circle of clear material, to the microscope objective. This blocking halved the effective period of the grating and greatly extended the depth of focus.

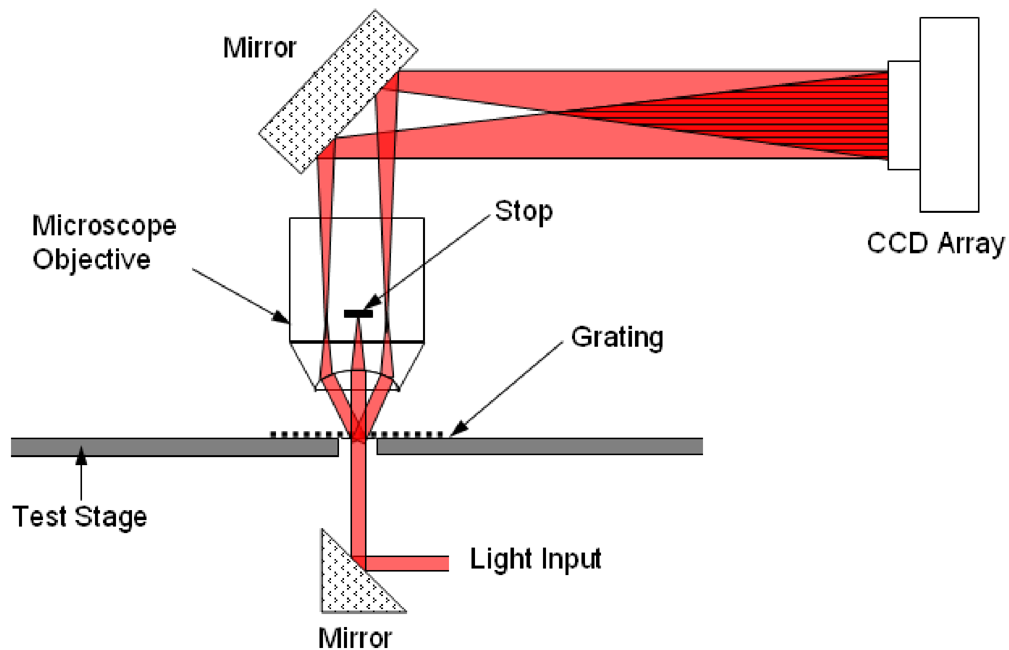

Figure 3.5 Optical system for detecting horizontal position of the stage (not to scale).

After passing through the microscope objective, the two first-order beams were reflected by another mirror and then projected to form a fringe pattern which is also an image of the grating on a CCD video array at a distance of about 50 cm. The expected magnification was approximately 125X which was calculated by dividing the distance between the microscope objective and the CCD camera (about 50 cm) by the focal length of the microscope objective (~ 4 mm).

$$Expected\ Magnification = \frac{500}{4} = 125 \tag{3.1}$$

The projected grating patterns were observed on a 9 inch TV screen (about 18 cm by 14 cm) by connecting the camera to the monitor. Figure 3.6 shows a typical in-focus fringe pattern on the monitor. The patterns on the screen were recorded on a VCR during the experiment and then analyzed off-line with a digital oscilloscope. The total horizontal scan of the video signal on the oscilloscope was 60 μsec. The fringe period on CCD array, 120 μm, was computed from the known width of the CCD array of 4.4 mm and the measured period of the video signal of the grating, 1.69 μsec, corresponding to 1.69/60 of the horizontal scan, or about 124 μm.

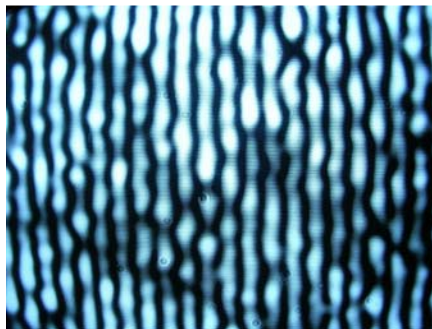

Figure 3.6 In-focus fringe pattern on TV monitor.

CCD array width : Fringe period on the CCD = Total scan : Measured grating period

4.4 mm : χ = 60 μsec : 1.69 μsec

$$\chi = \frac{1.69}{60} \times 4.4 = 0.124 \quad [\text{mm}] \tag{3.2}$$

The ratio between the image of the grating period on the CCD array, 124 μm, and the actual grating period, 2 μm, is 62. However, the projected image of the grating was reduced by a factor of 2 because the zero-order beam was blocked, halving the effective period of the grating. Therefore, the measured magnification of this optical system was about 124X, in good agreement with the expected magnification calculated above.

Motions parallel or perpendicular to the long dimension of the stage were measured with the lines in the diffraction grating aligned perpendicular or parallel to the long dimension, respectively. In each case the video array was rotated so that the image of the diffraction grating was displayed on a monitor as a series of vertical lines and spaces. This made all the horizontal video scan lines nominally identical, permitting them to be averaged by the oscilloscope. A typical video signal averaged over 128 consecutive scan lines.

CHAPTER 4

EXPERIMENTAL METHODS

4.1 Depth of Focus

The prototype stage was easily moved vertically after it was set just below the Euler's limit. Vertical motions were initiated by applying weights on the stage or by pulling it up with a spring. The height monitoring photodiode voltage was measured and converted to the vertical stage position using the vertical calibration data (Figure 3.4). The optical system imaged the diffraction grating to the CCD array (Figure 3.5). The fringe patterns on the monitor were observed and recorded during the entire vertical motions.

4.2 Resonant Frequency

The prototype stage was leveled by adjusting the screws at the right hand side around fulcrum (Section 3.1). This leveled condition corresponded to zero volts on the photodiode and a clear image of the grating projected on the CCD camera viewed by a monitor. After leveling, the vertical resonant frequency of the stage was measured by tapping the stage. The compressive loading was set just below the Euler's limit. Below the Euler's limit, higher compression resulted in a lower resonance frequency; however, above the Euler's limit, the compression resulted in an unstable stage snapping either above or below the median plane. Therefore, a minimum value of the frequency was obtained by increasing the compressive loading as much as possible before reaching the unstable state. During this experiment, the vibration was monitored on a digital oscilloscope displaying the voltage of the split photodiode as a function of time. The

vertical resonant frequency of the stage without compressive loading was also measured as a reference.

4.3 Vertical Stage Position vs. Horizontal Stage Position

To produce vertical motion of the stage, weights were placed on the stage, or the stage was pulled up by using a spring after leveling, as described earlier. At the same time, optical systems measured both vertical and horizontal movements. The split diode voltages were converted to vertical displacements by the calibration data (Figure 3.4). The fringe patterns on the CCD array were recorded and analyzed off-line with a digital oscilloscope that averaged 128 consecutive video scan lines (Figure 4.1). Time measurements were made between the horizontal sync pulse at the beginning of the video scan and the position of minimum intensity of the first 4 or 5 fringes in the video signal.

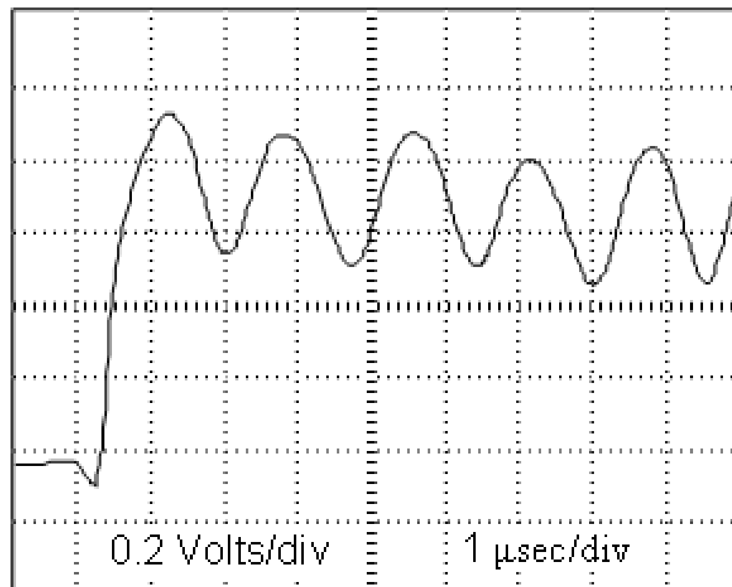

Figure 4.1 Typical averaged video signal, used to determine horizontal stage position.

4.4 Vertical Stiffness

The vertical movement of the stage was studied under the two conditions: i) with compressive force, and ii) with no compressive force. Weights were placed near the center of the stage (near the grating), and the photodiode voltages were measured with a digital voltimeter. This procedure was repeated several times, and the results were averaged. The averaged values were converted into stage displacements using the vertical stage calibration data, e.g. Figure 3.4.

4.5 Horizontal Stiffness

The transverse stiffness of both the uncompressed and compressed stage was measured as follows.

a. The stage was centered and the resonant frequency was set to about 8 Hz under the compressive force. The split photodiode was positioned so that its output voltage was zero with no external force. Its voltage range was observed to be about from - 67 mV to + 67 mV when the stage was moved from its lowest to highest level.
b. A pulley was used to apply horizontal forces at the midpoint of stage, roughly parallel to its long direction. The pulley was adjusted to minimize the vertical motion as measured with the split photodiode.
c. Five weights were first applied sequentially on the pulley, and then they were removed sequentially. The entire process was repeated several times.
d. During all the experiments, the fringe patterns were observed on the TV screen and recorded by a VCR to measure the horizontal motion of fringes.
e. These recorded fringe patterns were then analyzed with a digital oscilloscope that averaged the video signal over 128 consecutive scan lines (Figure 4.1). Time

measurements were made between the horizontal sync pulse at the beginning of the video scan and the position of minimum intensity of the first 4 or 5 fringes in the video signal.

f. The photodiode voltage was also measured to detect any undesired vertical displacements of the stage.

g. The measurements were repeated several times to achieve a more reliable experimental result.

h. Finally, the compressive loading was removed, and then the entire procedure (a ~ g) was repeated.

CHAPTER 5

RESULTS AND DISCUSSION

5.1 Depth of Focus

Alignment tracking optics should have large depth of focus to form sharp images of both the template and the substrate patterns during the whole imprint process. The theoretical value of the depth of focus of the tracking optics described here was 3 mm, which is sufficient gap between the template and substrate for most micro/nano device fabrication. Figure 5.1 shows the fringe patterns on the monitor during the stage's vertical motions of about 120 μm, showing that the images remain sharp. The increased depth of focus enables tracing the relative positions of the template and the substrate over the full range of motion of the stage and will help to enhance the alignment accuracy.

5.2 Resonant Frequency

Tapping the stage caused it to oscillate in the vertical direction. In the absence of a compressive load the resonant frequency of the stage was about 42 Hz. Figures 5.2(a) and (b) show oscilloscope traces of the height of the vibrating stage as recorded with the split photodiode with no compression at this frequency at different time scales. The oscillation decayed with about a 3 second time constant (Figure 5.2b).

The application of an in-plane compressive load greatly reduced both the resonant frequency and the decay time. Resonant frequencies below 8 Hz were routinely obtained; the lowest resonant frequency observed was about 5 Hz. Figure 5.2(c) shows an oscilloscope trace at a frequency of 6 Hz under compressive load. The decaying time observed was about 360 msec.

(A) 58.0 μm

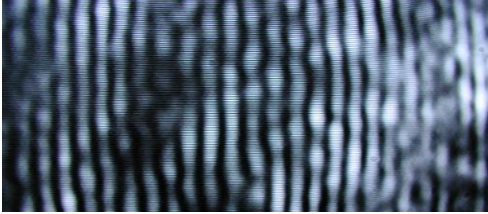

(B) 39.4 μm

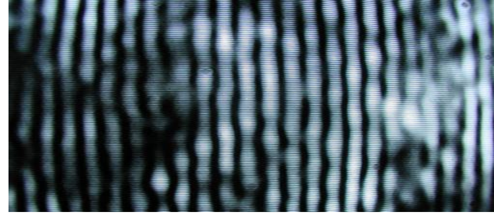

(C) 21.4 μm

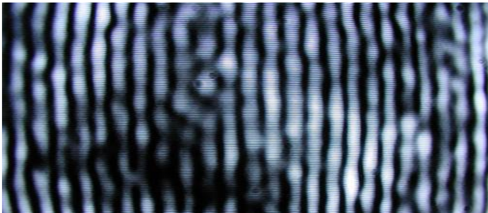

(D) 9.6 μm

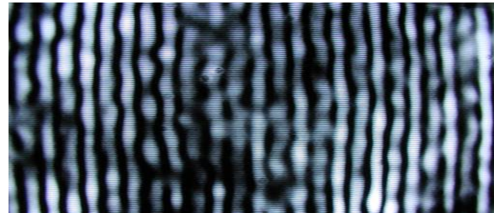

(E) -15.2 μm

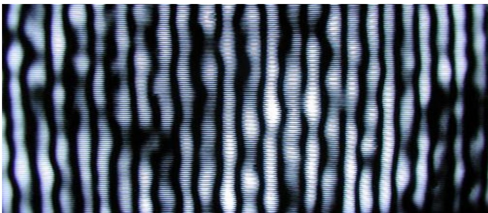

(F) -34.0 μm

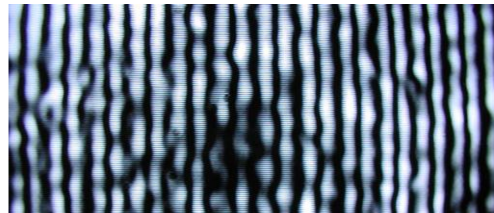

(I) -60.8 μm

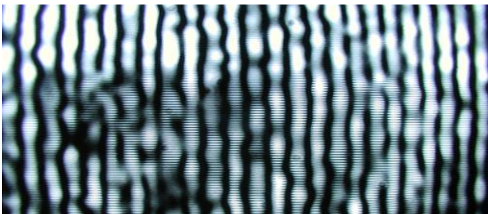

Figure 5.1 Fringe patterns on the monitor over the stage's vertical motion of about 120 μm.

From Equation 2.2, a reduction in frequency of vertical oscillation of the stage, f, by a factor of α corresponds to a decrease in the vertical spring constant, k, by α^2, because the effective mass of the stage remains the same. In the case of the resonant frequency of 42 Hz for the uncompressed stage and that of 6 Hz for the compressed stage, the vertical spring constant was decreased by a factor of about 49. This result implies that the compressive load decreased the vertical spring constant of the stage resulting in high vertical compliance.

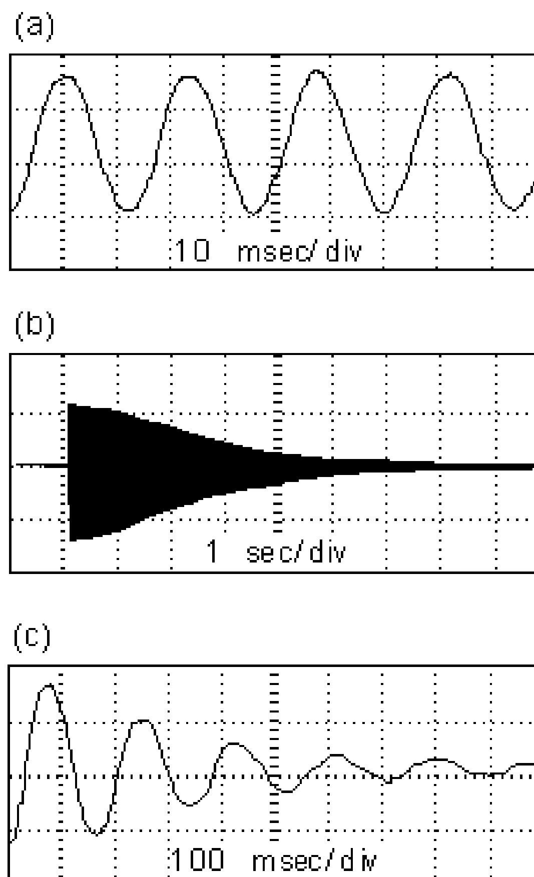

Figure 5.2 Vertical stage oscillations. (a) and (b), Vibrations observed with no compression on the stage. The scales of (a) are 10 msec/div in horizontal and 20 mV/div in vertical, and those of (b) are 1 sec/div in horizontal and 50 mV/div in vertical. (c) Stage compressed, increasing the period and decreasing the decay time of the oscillations. The horizontal scale is 100 msec/div, and the vertical scale is 20 mV/div.

The decreased amount of the spring constant also can be seen in similar analysis. The potential energy, U, stored in a spring, e.g., the prototype stage, is given by

$$U = \frac{1}{2} K x^2 \tag{5.1}$$

where K is the spring constant and x is the extended length. For a given extended length, the energy is proportional to K. As the spring oscillates, the stored energy decreases due to its internal friction. The fraction of the energy lost per cycle is approximately constant, and the amplitude of oscillation decays exponentially. Consequently, number of cycles should be proportional to the spring constant, K, or the square of the frequency, f^2.

From the experiments, the number of cycles for the vibration of the uncompressed stage to decrease by a factor of e was 126 at a frequency of 42 Hz and a decay time of 3 sec. For the compressed stage, the number of cycles was about 2.16 at a frequency of 6 Hz and 0.36 sec decay time. The ratio of the number of cycles between the uncompressed and compressed stages is 58. This ratio implies that the spring constant of the compressed stage is reduced by a factor of 58, in fair agreement with the measured square of the frequencies, 49.

Similarly, the ratio of the stages' decay times is expected to be proportional to the ratio of their frequencies. If the decay time and frequency of the uncompressed stage are T_1 and f_1, and those of the compressed stage are T_2 and f_2, then

$$\frac{T_1 \times f_1}{T_2 \times f_2} \approx \frac{K_1}{K_2} \approx \frac{f_1^2}{f_2^2}$$

$$\frac{T_1}{T_2} \approx \frac{f_1}{f_2}$$

$$8.3 \approx 7.0 \tag{5.2}$$

5.3 Vertical Stage Position vs. Horizontal Stage Position

As the stage moved vertically, an apparent horizontal motion caused small shifts in the video scan lines stored in the digital oscilloscope. The separation between minima corresponds to a horizontal motion of 1 μm; the measured value was about 1.69 μsec (Figure 4.1). Table 5.1 shows the measured vertical position of the stage and the periods of the first 5 minima in the averaged video signal.

The averaged one period, P, at each vertical position was calculated by subtracting x_1 from x_5 and then dividing them by 4, and the results can be seen in Table 5.2. Next, the averaged period P, 2P, and 3P were subtracted from each time measurements, x_1, x_2, x_3, and x_4. The average and standard deviation of them were obtained in Table 5.2. The time measurements were converted to the micron scale, i.e., horizontal position, by dividing them by P (Table 5.3). The averaged value of each standard deviation was ±16 nm, and averaging 4 fringes improved the accuracy by a factor of 2 resulting in an accuracy of ± 8 nm.

Figure 5.3 shows the horizontal position of the stage over a vertical range of about 120 μm. It should be noted that the apparent small change in horizontal position is not an actual horizontal motion; it is an artifact caused by the reference laser beam being not exactly vertical. What is significant is that the points lie accurately on a straight line and that horizontal position of the stage at any height can be extrapolated from its position at any other height.

5.4 Vertical Stiffness

Figure 5.4 shows the vertical displacement of the stage as a function of the applied force for the compressed and the uncompressed stage. The solid circles represent

Table 5.1 Measurements of the vertical position of the stage and the time measurements of the video signal.

Vertical		Horizontal – Time measurements				
Voltage (mV)	Position (μm)	x_1 (μsec)	x_2 (μsec)	x_3 (μsec)	x_4 (μsec)	x_5 (μsec)
29.0	58.0	1.52	3.28	4.96	6.68	8.36
19.7	39.4	1.56	3.24	4.96	6.64	8.32
10.7	21.4	1.64	3.32	5.04	6.76	8.44
4.8	9.6	1.64	3.32	5.04	6.76	8.44
-7.6	-15.2	1.68	3.40	5.08	6.72	8.40
-17.0	-34.0	1.76	3.44	5.04	6.88	8.48
-30.4	-60.8	1.80	3.48	5.20	6.80	8.44

Table 5.2 Averaged one period, P, and analysis of time measurements data at every vertical position of the stage.

Vertical Position (μm)	Time Measurements (μsec)						
	P	x_1	x_2-P	x_3-2P	x_4-3P	Average	Stdev
58.0	1.71	1.52	1.57	1.54	1.55	1.545	0.021
39.4	1.69	1.56	1.55	1.58	1.57	1.565	0.013
21.4	1.70	1.64	1.62	1.64	1.66	1.640	0.016
9.6	1.69	1.64	1.63	1.66	1.69	1.655	0.026
-15.2	1.68	1.68	1.72	1.72	1.68	1.700	0.023
-34.0	1.69	1.76	1.75	1.66	1.81	1.745	0.062
-60.8	1.67	1.80	1.81	1.86	1.79	1.815	0.031

Table 5.3 Conversion of the time measurements to the stage's horizontal position.

Time (usec)		Position (μm)	
Average	Stdev	Average	Stdev
1.545	0.021	0.903509	0.012173
1.565	0.013	0.926036	0.007639
1.640	0.016	0.964706	0.009606
1.655	0.026	0.97929	0.015655
1.700	0.023	1.011905	0.013746
1.745	0.062	1.032544	0.036953
1.815	0.031	1.086826	0.018618
Average		0.986402	0.016341

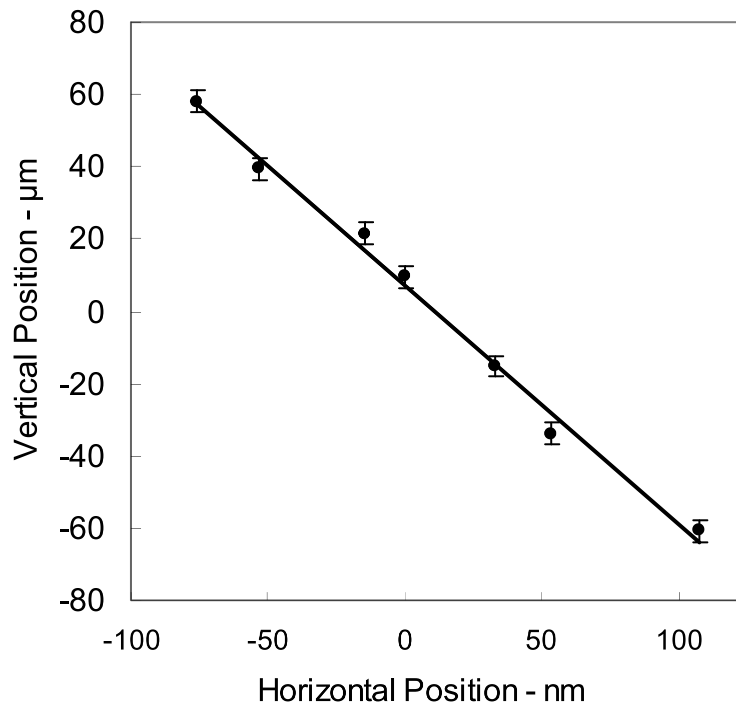

Figure 5.3 Change in horizontal position as the stage is moved vertically.

the compressed stage while the clear circles are for the uncompressed stage. As can be seen, the application of an in-plane compressive load dramatically reduces the force needed for vertical deflection. For example, the vertical displacement of the uncompressed stage was only 2.1 μm at 6.18 grams with a slope of about 0.3 μm/gram; however, that of the compressed stage was about 60 μm, with a slope of approximately 9.0 μm/gram. In other words, the compressive load reduced the stage's vertical stiffness, from a value of 3.3 grams/micron to 0.1 grams/micron for a stage with a resonant frequency of about 6 Hz. Each data points can be seen in Table 5.4.

The above experimental result was in fair agreement with theory. For example, when the resonant frequency is reduced by a factor of 7 (from 42 Hz to 6 Hz) by applying a compressive load, the vertical spring constant, Kv, decrease by 49, according to equation 2.2. Since the vertical spring constant is directly proportional to vertical stiffness, the compressed stage is 49 times less stiff than the compressed stage theoretically. The measured stage stiffness was reduced by a factor of about 33, from 3.3 grams/micron to 0.1 grams/micron. It is possible that the application of weights might produce residual stress in the stage, causing subtle changes in frequency during the experiments, resulting in the discrepancy between the theoretical and experimental values.

5.5 Horizontal Stiffness

Figure 5.5 shows the horizontal displacement of the compressed and uncompressed stage as a function of applied horizontal force (weights), and each data points can be seen in Table 5.5. The solid circles represent the compressed stage; the

clear ones are the uncompressed stage. The horizontal stiffness was about 4,000 grams/micron under compressive loading, slightly less than 5,600 grams/micron observed

Table 5.4 Vertical displacements of the compressed & the uncompressed stage at different vertical force.

Force in weights [grams]	Vertical Displacements [μm]	
	Compressed Stage	Uncompressed Stage
0.00	0.0	0.0
2.06	19.3	0.8
4.12	39.5	1.5
6.18	59.3	2.1
8.24	77.7	2.9
10.30	91.1	3.6

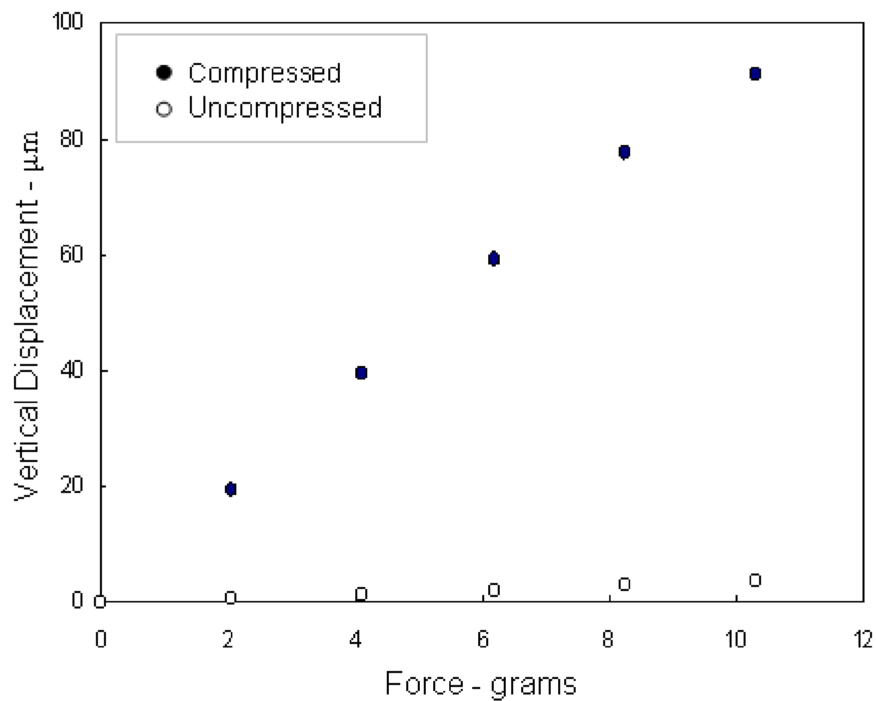

Figure 5.4 Vertical displacements as a function of applied force in grams weight.

unloaded. However, the observed horizontal stiffness of the compressed stage was about 40,000 times greater than the vertical stiffness, which was about 0.1 grams/micron, while that of the uncompressed stage was only greater about 1,700 times than the vertical stiffness. As expected, the stage was more compliant in the horizontal direction perpendicular to its long dimension, deflecting about 3 μm/kilogram of weight for both loaded and unloaded conditions.

Although the proposed stage is very stiff horizontally, an even stiffer stage can be achieved by changing the stage's dimensions. From the definitions on page 2, the stress, σ, and the stiffness, *k*, can be defined as

$$\sigma = \frac{F}{A} = \mathrm{E}\varepsilon = \mathrm{E}\frac{\Delta L}{L}$$

$$F = \frac{\mathrm{E}A\Delta L}{L}$$

$$k = \frac{F}{\Delta L} = \frac{\mathrm{E}A}{L} \tag{5.3}$$

where F is the applied force, A is the cross-sectional area of the stage, E is Young's modulus, L is the original length of the stage, and ΔL is the extended length. Therefore, a larger cross-section area and a shorter length of the stage can be used to produce a horizontally stiffer stage. Unfortunately, this change will also increase the vertical stiffness of the stage; however, the compressive load at Euler's limit can be applied on the stage to improve the vertical compliance while maintaining most of the horizontal stiffness.

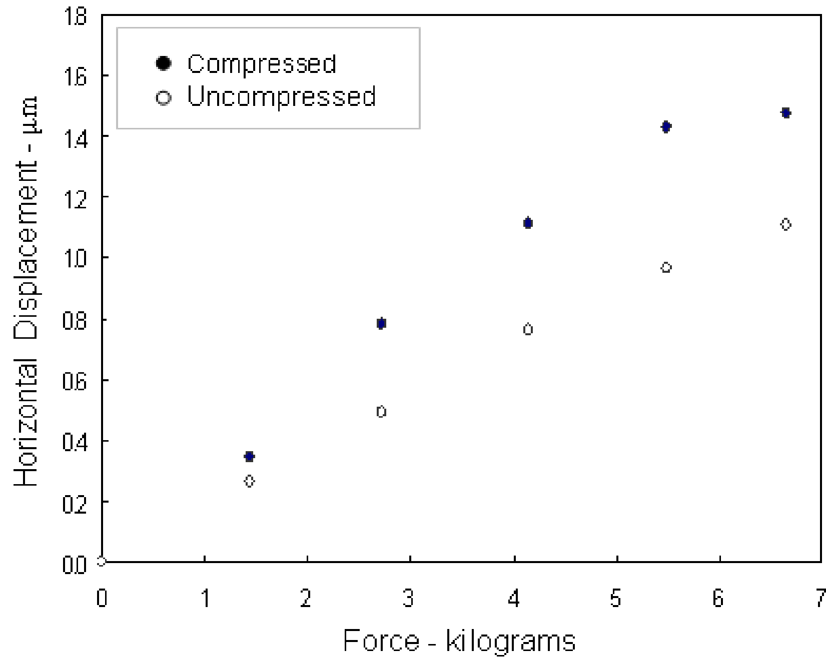

Figure 5.5 Horizontal displacements as a function of applied force parallel to the stage in kilograms weight.

Table 5.5 Horizontal displacements of the compressed & the uncompressed stage at different horizontal force.

Force in weights [Kilograms]	Horizontal Displacements [µm]	
	Compressed Stage	Uncompressed Stage
0.00	0.00	0.00
1.44	0.35	0.27
2.72	0.78	0.49
4.14	1.12	0.76
5.50	1.43	0.96
6.66	1.48	1.11

CHAPTER 6

CONCLUSIONS

Nanoimprint and step-and-flash lithography have attracted great attention as the next generation lithography due to their excellent resolution, high throughput, and low cost. However, several issues still need to be addressed to adopt these techniques to the silicon IC industry: stamp fabrication, polymer issues, residual layer control, accurate alignment, developing suitable tools, system automation, and so on. In this thesis, a lithographic tool with high alignment capability has been demonstrated.

A prototype imprint stage has been demonstrated with extremely high transverse stiffness and relatively free motion in vertical direction. A compressive load slightly below the Euler's limit was applied to the stage, resulting in easy vertical motion over hundreds of microns while maintaining most of the stage's horizontal stiffness. From the experiments, the vertical and horizontal stiffness of the natural stage were measured about 3.3 grams/µm and 5.6 kg/µm, respectively, both at a resonant frequency of 42 Hz; however, those of the compressed stage were measured as 0.1 grams/µm and 4.0 kg/µm both at 6 Hz, respectively. Fortunately, the higher vertical compliance will be achieved when the force is even closer to the Euler's limit.

The imprint stage reduces some serious sources of misalignment during the process and satisfies important requirements of the lithographic tools. First, the high horizontal stiffness of the stage decreases mechanical shifts between template and substrate. In imprint lithography, large forces at contact often produced unwanted

sideway stresses on the template, which lead to misalignment or imprint failure. In addition, the horizontal was measured to about ± 8 nm over the vertical motion of about 120 μm. Consequently, the template and substrate atterns can be observed and adjusted during the whole imprint process, reducing any misalignment errors arisen from the process.

Although this prototype is already quite stiff, far stiffer stages could be constructed using more optimal geometries. For example, the horizontal stiffness is linearly proportional to the cross-sectional area of the flexing part of the stage, which was only 1.5 cm^2. As discussed, two relatively wide slabs joined at right angles would provide high stiffness in all horizontal directions (Figure 2.4).

Lastly, the reproducibility of the stage simplifies demolding issues by bringing the template stage vertically back to its original position. This exact vertical motion of the stage minimizes the stress on any structures in a device, resulting in higher yield as many imprint failures occur during the demolding step. However, other critical parameters, such as relative thermal expansions and temperature gradients, will have to be carefully controlled.

BIBLIOGRAPHY

[1] D. J. Resnick, et. al., Imprint lithography for integrated circuit fabrication, J. Vac. Sci. Technol. B 26(6), Nov/Dev 2003, pp 2624-2631.

[2] Colin Stuart, et al., Nanofabrication module integrated with optical aligner, J. Vac. Sci. Technol. B 24(2), Mar/Apr 2006, pp.539-542

[3] B.J. Choi, et al., Layer-to-Layer Alignment for Step and Flash Imprint Lithography, Proc. SPIE Vol. 4343, p. 436-442, 2001

[4] B.J. Smith, et al., Employing Step and Flash Imprint Lithography for Gate Level Patterning of a MOSFET Device, Proc. SPIE Vol. 5037, pp.1029-1033, 2003

[5] www.molecularimprints.com

[6] Wei Zhang and Stephen Y. Chou, Multilevel nanoimprint lithography with submicron alignment over 4 in Si wafers, Applied physics letters, vol. 79, number 6, pp. 845-847, 2001

[7] Li Jiang and Martin Feldman, Accurate alignment technique for nanoimprint lithography, Proceedings of SPIE, vol.5752, May 2005, pp.429-437

[8] Li Jiang, A dissertation: Integrated circuit metrology by multilevel patterning technology, May 2006. Louisiana State University.

[9] Model TDS 210, Tektronix Inc., 14200 SW Karl Braun Drive, Beaverton, OR 97077

[10] Model 47257-5VGA, Harbor Freight Tools, 3491 Mission Oaks Blvd., Camarillo, CA 93011.

VITA

Yunmi Jeon was born in Busan, South Korea, on April 23, 1982. She earned her Bachelor of Science degree in electrical & computer engineering, at Dong-A University, Busan, South Korea, in February 2005. Her major area was electronics. She was enrolled in Department of Electrical & Computer Engineering, Louisiana State University, Baton Rouge, Louisiana, in August 2005. She is currently a doctoral candidate, and expects the degree of Master of Science in Electrical Engineering in December 2007.